Numerical evidence for robustness of environment-assisted quantum transport

A. Shabani,[1,*] M. Mohseni,[2,*] H. Rabitz,[1] and S. Lloyd[3]
[1]*Department of Chemistry, Princeton University, Princeton, New Jersey 08544 USA*
[2]*Center for Excitonics, Research Laboratory of Electronics, Massachusetts Institute of Technology, Cambridge, Massachusetts 02139 USA*
[3]*Department of Mechanical Engineering, Massachusetts Institute of Technology, Cambridge, Massachusetts 02139 USA*
(Received 22 December 2013; published 15 April 2014)

Recent theoretical studies show that decoherence process can enhance transport efficiency in quantum systems. This effect is known as environment-assisted quantum transport (ENAQT). The role of ENAQT in optimal quantum transport is well investigated; however, it is less known how robust ENAQT is with respect to variations in the system or its environment characteristic. Toward answering this question, we simulated excitonic energy transfer in Fenna-Matthews-Olson photosynthetic complex. We found that ENAQT is robust with respect to many relevant parameters of environmental interactions and Frenkel-exciton Hamiltonians, including reorganization energy, bath-frequency cutoff, temperature, initial excitations, dissipation rate, trapping rate, disorders, and dipole moments orientations. Our study suggests that the ENAQT phenomenon can be exploited in robust design of highly efficient quantum transport systems.

DOI: 10.1103/PhysRevE.89.042706 PACS number(s): 82.39.Rt, 63.20.kk, 71.35.−y, 03.65.Yz

I. INTRODUCTION

Quantum and coherent transport are common phenomena in many natural and artificial systems [1–3]. In a quantum system, transfer of matter and energy is strongly influenced by structural disorder and environmental noise. Recently, it was discovered, in the context of energy transfer in photosynthetic complexes, that environmental interactions can have a constructive role in excitonic transport, called ENAQT effect [3–12]. Basically, a decoherence process can facilitate excitons displacement between molecules by breaking wavefunction localization [5,7], energy-level broadening [8,9], or quantum jumps [4,10]. Based on ENAQT theory, optimal quantum transport is achieved by an optimal interplay of the system coherence and decoherence dynamics, influenced by the environment structure [11,12]. The convergence of system-environment energy scales is an underlying principle for such an optimal transport process [4].

In this paper, we study the role of ENAQT in the robustness of quantum transport, a feature complement to optimality. To this end, as a model system, we consider excitonic energy transfer in Fenna-Matthews-Olson (FMO) complex and investigate the efficiency of transport in the presence of large variations in internal and external conditions. The FMO complex is a trimer consisting of three identical monomers, each formed from seven bacteriochlorophylls (BChl) embedded in a scaffold protein. An FMO unit acts as an energy transfer channel in green sulfur bacteria, guiding excitons from the light-harvesting antenna complex to the reaction center. Recent electronic spectroscopy experiments provide evidence that long-lived quantum dynamical coherence can exist in FMO complex [13–17]. Such experimental observation suggests that modeling excitonic dynamics requires describing FMO as an open quantum system to include both the internal coherence and the decoherence induced by the protein scaffold environment.

For our modeling, we employed the time-convolutional master equation (TC2) that we derived and analyzed in Ref. [18]. In our study, we consider the environmental parameters, including reorganization energy, bath-cutoff frequency, temperature, and trapping. The role of antenna complex is studied by varying the initial excitonic states and its impact on energy-transfer efficiency (ETE). For the internal parameters, we study the robustness of ETE in presence of disorder in the FMO internal structure parametrized by site energies, interchlorophyl distances, and dipole moment orientations. We observe that ENAQT enhances robustness of energy transfer while it is a universal phenomenon in the sense that the environment can assist transport even at nonoptimal regime of parameters.

The results presented in this manuscript are part of an extensive study; we have reported on other aspects of this study in Refs. [7,18,19]. A new derivation of the TC2 master equation along with assessment of its reliability for calculating energy transfer efficiency beyond perturbative and Markovian limits was presented in Ref. [18]. Reference [7] presents an underlying principle, the convergence of system and environment energy scales to describe optimal quantum transport. We discussed the role of geometrical character of an excitonic system in energy transfer in Ref. [19]. The current study presents numerical evaluation of robustness for the ENAQT phenomenon, while our previous papers [7,18,19] address the role of ENAQT as an enhancement of energy transfer.

II. THEORETICAL MODEL

The FMO electronic states at low-energy limit is modeled as a seven-level quantum system (Fig. 1) with Hamiltonian

$$H_S = \sum_{j,k} \epsilon_j |j\rangle\langle j| + J_{jk}|j\rangle\langle k|, \tag{1}$$

where $|j\rangle$ denotes an excitation state in a chromophore spatially located at site j. The diagonal site energies are denoted by ϵ_js. The strengths of dipole-dipole interactions between chromophores in different sites are represented by J_{jk}. We model the protein scaffold as a bath of harmonic

*Current address: Google Inc., 340 Main St, Venice, CA 90291.

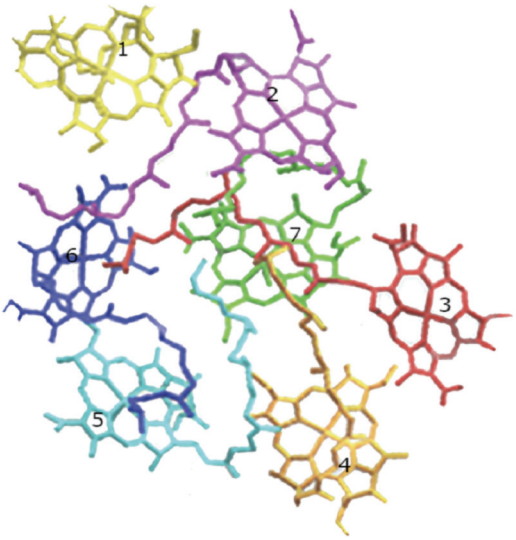

FIG. 1. (Color online) The disordered structure of the Fenna-Matthews-Olson (FMO) complex. Seven BChls are embedded in a protein scafold that is modeled as a bath of harmonic oscillators. Initial exciton is usually formed on BChls 1 and 6, which are in the proximity of light-harvesting antenna complex, and is transferred to the reaction center, which is in the proximity of BChls 3 and 4.

oscillators with Gaussian fluctuations [20]. Each BChl is coupled to a separate bath with interaction Hamiltonian $H_{SB} = S_j B_j$ where $S_j = |j\rangle\langle j|$, and B_j is the jth bath operator. We assume a Drude-Lorentzian correlation function, given at temperature T as

$$C_j(t) = \langle \tilde{B}_j(t)\tilde{B}_j(0)\rangle = \frac{1}{\pi}\int_0^\infty d\omega J(\omega)\frac{\exp(-i\omega t)}{1-\exp(-\hbar\omega/k_B T)}, \quad (2)$$

where the spectral function has the form $J(\omega) = 2\lambda\omega/(\omega^2 + \gamma^2)$. For FMO, we considered the reorganization energy value of $\lambda = 35\ \mathrm{cm}^{-1}$ and bath cutoff frequency $\gamma = 50\ \mathrm{cm}^{-1}$, all the same for different BChls.

In order to model the FMO electronic degrees of freedom as an open quantum system, we employ the time-nonlocal master equation TC2:

$$\frac{\partial}{\partial t}\rho(t) = \mathcal{L}_S\rho(t) + \mathcal{L}_{e-h}\rho(t) - \sum_j \left[S_j, \frac{1}{\hbar^2} \times \int_0^t C_j(t-t')e^{\mathcal{L}_S(t-t')}S_j\rho(t')dt' - \mathrm{H.c.}\right], \quad (3)$$

where the $\mathcal{L}_S = -i[H_S,.]$. Here, we include the effect of exciton loss and reaction center (RC) trapping by the superoperator $\mathcal{L}_{e-h} = -\sum_j r^j_{\mathrm{loss}}\{|j\rangle\langle j|,.\} - r_{\mathrm{trap}}\{|\mathrm{trap}\rangle\langle\mathrm{trap}|,.\}$. In the first term, the loss rate is $r^j_{\mathrm{loss}} = (1\,\mathrm{ns})^{-1}$ while the second term $r_{\mathrm{trap}}\{|\mathrm{trap}\rangle\langle\mathrm{trap}|,.\}$ represents the exciton capturing process by the reaction center. We consider BChl3 as the trapping site with the trapping rate of $r_{\mathrm{trap}} = (0.5\,\mathrm{ps})^{-1}$.

We quantify ETE as the total portion of a traveling exciton successfully captured by the reaction center:

$$\eta = 2r_{\mathrm{trap}}\int_0^\infty \langle\mathrm{trap}|\rho(t)|\mathrm{trap}\rangle dt. \quad (4)$$

The above performance function had been used in our previous studies [4,7,18,19]. In Ref. [18], we examined that TC2 equation provides reliable estimation of ETE for the range of parameters considered in this study.

III. ROBUSTNESS WITH RESPECT TO ENVIRONMENTAL PARAMETERS

We examine the degree of optimality and robustness of the energy transfer by employing the Euclidean norm of the gradient and Hessian matrix of the ETE function. The Euclidean norm of the ETE gradient at any parameters values p_1 and p_2, $||\nabla\eta(p_1,p_2)||_2$, quantifies the degree of optimality. The gradient measure reveals the degree of local optimality in a surface manifold. Careful inspections of the room temperature plots for the ETE function versus various pairs of relevant parameters show a convex or concave manifold, thus gradient as a measure of local optimality suffices to measure global optimality. To examine the robustness, we compute the Hessian matrix norm $||H(\eta(p1,p2))||_2 = ||[\partial^2\eta/\partial p_i\partial p_j]||_2$ $(i,j = 1,2)$ as the total measure of local curvature of the manifold. A smaller value of this norm corresponds to a flatter surface, thus a more robust process. We use a five-point stencil method to compute derivatives numerically.

A quantitative study of the degree of optimality and robustness of the energy transfer as functions of system-bath coupling strength and bath memory is illustrated in Fig. 2. The optimality is defined as Euclidean norm of the ETE function gradient $||\nabla\eta(\lambda,\gamma)||_2$ to locate the local maxima in the ETE landscape in Fig. 2. The robustness is defined by $||H(\eta(\lambda,\gamma))||_2$ to measure local curvature of the manifold. Note that the ETE gradient and Hessian matrix norms are indicated in a logarithmic scale, thus the global optimal point with zero derivative cannot be explicitly highlighted in this representation. The experimentally estimated values for FMO are illustrated as black dots in each graph clearly located in an optimal and robust region. One remarkable feature is the fact that environmental parameters of FMO have almost the minimal reorganization energy and bath cutoff frequency among all the regions with simultaneous optimal and robust properties. One hypothetical explanation could

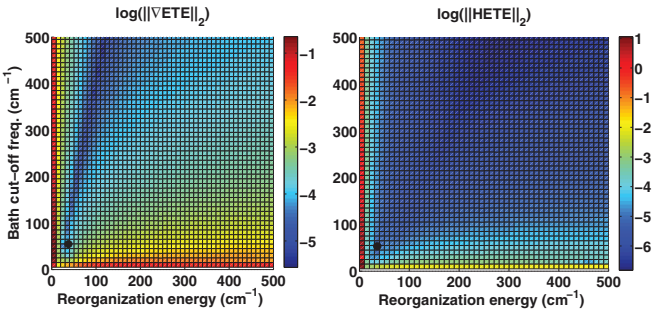

FIG. 2. (Color online) Left: The degree of ETE optimality is quantified at different values of λ and γ by the gradient matrix norm of the ETE function. The dark blue points represent near optimal values. Right: The degree of ETE robustness is quantified by the Euclidian norm of Hessian of the ETE. The dark blue points represent near robust points. The estimated FMO environmental values of $\lambda = 35\,\mathrm{cm}^{-1}$ and $\gamma = 50\,\mathrm{cm}^{-1}$, marked by black dots, are located on the corner of both robust and optimal region.

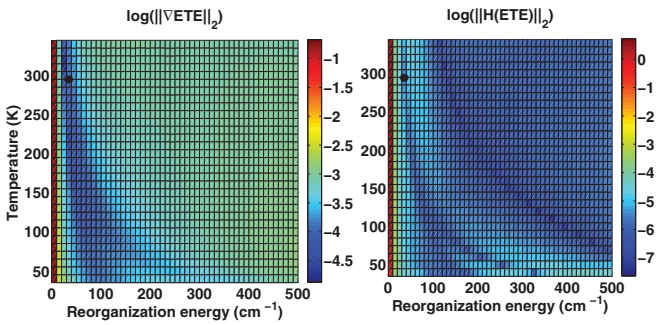

FIG. 3. (Color online) Left: the degree of ETE optimality is quantified at different values of λ and T by the norm of the ETE gradient. The dark blue points represent near optimal values. Right: the degree of ETE robustness is quantified by the Euclidian norm of the ETE Hessian. The dark blue points represent near robust points. We note that within the range of possible FMO operating temperatures (e.g., between $T = 280°$K and $T = 350°$K) simultaneous optimal and robust energy transport can only be achieved for λ values around 30 to 35 cm^{-1}, which is equivalent to the estimated reorganization energy for the FMO complex that is marked by a black dot at room temperature $T = 298°$K.

be the overall tendency in nature to minimize the amount of required work, that is, facilitating an optimal and robust environmental platform for the FMO energy transport by preserving a rather small-size scaffold protein that is weakly coupled. However, one may ask why nature has not evolved toward an even more compact complex. On reason could be that pigments at closer distances can exchange electrons in addition to excitons that would reduce the excited state lifetime, the so-called concentration quenching. However, using the modeling considered in this paper we are not able to examine such a hypothesis.

The gradient and Hessian norms as functions of reorganization energy and temperature are illustrated in Fig. 3. At the relevant FMO operating temperatures, optimum and robust energy transport can occur simultaneously only within a small region of λ between 30 to 35 cm^{-1}, which coincide with the estimated values of reorganization energy for the FMO. We note that there are certain regions of higher robustness at higher reorganization energy that are in principle available, but these regions imply a significantly lower operating temperature for the FMO operation and they have suboptimal ETE in comparison with actual FMO environmental parameters at the room temperature. The robustness with respect to environmental parameters had been previously reported in Refs. [7,18,21] but with no direct quantification of robustness and mere graphical observation.

IV. ENERGY TRANSPORT SENSITIVITY ON THE INITIAL EXCITATIONS

The exciton migration pathways and time-scales have been studied in detail for a variety of light-harvesting complexes using various perturbative techniques including Förster models for studying LHI and II of purple bacteria [22] and Lindblad models for simulating the dynamics of the FMO protein of green sulfur bacteria [4]. Nevertheless, the role of initial conditions in the overall energy transfer efficiency of photosynthetic complexes is to a large extent unknown. It was recently shown that the initial quantum coherence could influence the energy transfer efficiency in LHI of purple bacteria, assuming no interaction with the phonon bath [10]. The dependency on initial localized excitation at BChls 1 and 6 were also examined for the FMO complex using Lindblad, Haken-Strobl, and HEOM models [4,6,23,24]. However, the sensitivity of ETE with respect to generic initial pure and mixed states taken from a large ensemble in the single-excitation manifold has not previously been explored.

Here, we first examine the average sensitivity of ETE with respect to randomly chosen initial states for various reorganization energies. To this end, for each value of reorganization energy, we sample over 10^4 (pure or mixed) density matrices from a uniform distribution in the space of all 7×7 trace one positive matrices. In Fig. 4(a) the average values of ETE is plotted with an error bar representing the variance of ETE in our random sampling. Note that at the optimal ETEs, corresponding to the value of reorganization energy of the FMO complex, the dependency of the variances on initial states is very small—less than 0.1%. However, the ETE fluctuations can grow by an order of magnitude for larger or smaller values of λ. We also investigate the best and worst possible random

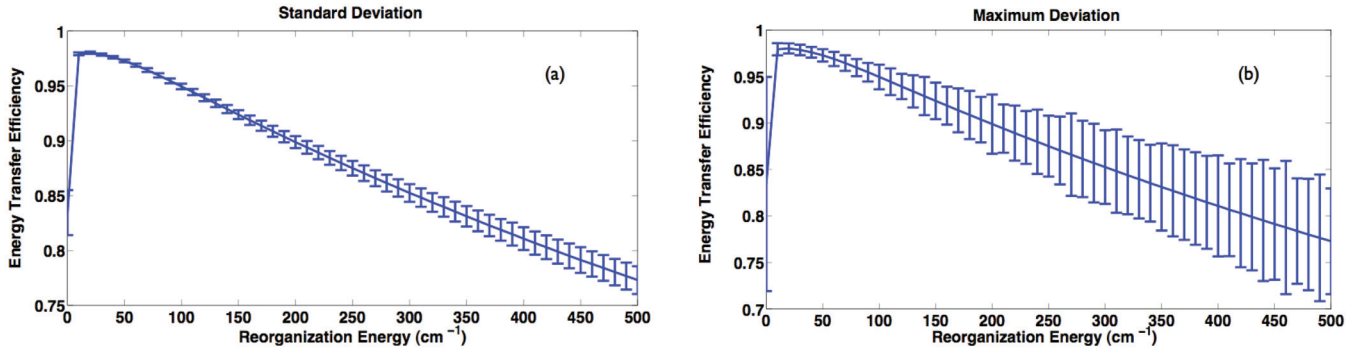

FIG. 4. (Color online) The degree of sensitivity of ETE for 10^4 uniformly sampled pure and mixed initial exciton density matrices for different values of reorganization energy: (a) The error bars indicate the ETE standard deviation. At the FMO value of $\lambda = 35$ cm^{-1} the standard deviation of ETE has a negligible value of about 0.1%. (b) A worst-case scenario of FMO energy transport sensitivity to initial exciton states. Here, the error bars indicate the maximum and minimum values of ETE achieved over the sample of 10^4 randomly chosen initial states. This plot clearly shows how ENAQT significantly reduces the dependence of ETE on the initial state of dynamics.

initial single excitonic states in the Hilbert space of FMO. In Fig. 4(b), we illustrate these extreme possible deviations by error bars on the average ETE at any given value of λ. Note that ETE is very robust, varying about 1% with respect to different initial excitations at the optimal area of ETE landscape. However, this robustness diminishes substantially at the regimes of large reorganization energy. Next, we study the ETE landscape as a function of trapping and dissipation rates.

V. TEMPORAL AND GEOMETRICAL EFFECTS OF THE TRAPPING MECHANISM

Basic structural information on the FMO-RC complex has been obtained via linear dichroism spectra and electron microscopy [25]. These studies indicate that the symmetry axis of the trimer is normal to the membrane containing the reaction center. The electron microscopy resolution is generally not sufficient to distinguish the top and the bottom of the FMO trimer nor the distance between FMO-RC. Thus, in principle, either pairs of BChls 1 and 6 or BChls 3 and 4 are the pigments that connect the FMO complex to RC. However, it is widely believed, due to efficient energy funneling toward RC, that BChl 1 and 6 are the linkers to antenna baseplate, and 3 and 4 should serve as target regions within the neghiborhood of RC complex [26]. This hypothesis has been recently verified experimentally [27]. Up to this point, we have considered BChl 3 to be in the close proximity of RC by a trapping time-scale of about 1 ps. However, in this section we consider both of these parameters to be free, in order to explore the optimality and robustness of the ETE landscape as we vary the time scale and geometrical constraints set by the RC trapping mechanism.

In Fig. 5, we study the behavior of energy transfer efficiency landscape in various trapping time-scales and reorganization energies. It is evident that as the trapping rate becomes very slow comparable to 100 ps or slower, the ETE drops significantly independent of the values of λ. This can be understood intuitively as follows: the excitation has to wait on average so long for successful trapping to take place

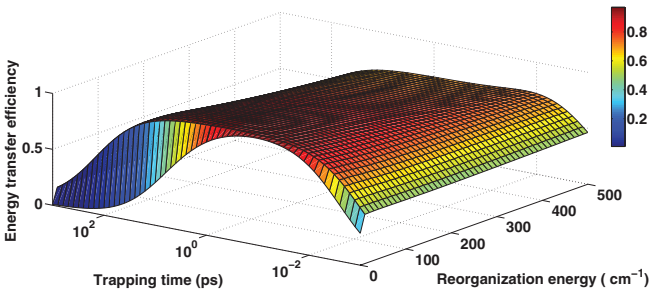

FIG. 5. (Color online) The ETE manifold on the parameter space of reorganization energy and trapping time scale. It can be seen that the FMO complex reaches its maximum functionality at trapping rates of about 0.5–5 ps^{-1}. The tunnel-shape ETE landscape can be understood by noting that at low trapping rates the transport efficiency is diminished by the recombination process. At high trapping rates the exciton transfer is suppressed via quantum Zeno effect as the trapping process corresponds to very strong and continuous measurement of the system.

such that there will be an increasing chance of electron-hole recombination as we are approaching time scales comparable to exciton lifetime. If the trapping mechanism occurs within a time scale of 1 ps, the ETE reaches to its expected maximum value of about 99%. Generally, one might expect that with increasingly faster trapping mechanisms the likelihood of dissipation to environment vanishes and energy transport approaches to the ideal case of having perfect efficiency. However, when the trapping rate becomes very fast on the order of 10^{-2} ps or faster, the ETE also drops significantly, a result that might appear counterintuitive. In fact, overly rapid trapping leads to low efficiency via the quantum Zeno effect, as the rapid trapping effectively freezes the exciton dynamics and prevents it from entering the reaction center. As a result, the finite exciton lifetime eventually leads to complete dissipation of excitation to the environment in extreme limit of fast trapping of about 1 fs.

The optimality and robustness of ETE versus both decoherence and trapping rates using gradient and Hessian norms are presented in Fig. 6 (left panel). It can be observed that at $\lambda = 35$ cm^{-1} for the FMO, the ETE is optimal with a trapping rate of about 0.5 ps. If the environmental interactions were stronger, a comparably faster trapping mechanism would be required to preserve such a high level of efficiency. However, for small and intermediate system-bath interaction strength, where environment-assisted transport occurs, slower trapping rates become optimal, that is λ and r_{trap} are not competing processes anymore. This implies that a multiparameter convergence of time scales of the relevant physical processes might be required for light-harvesting complexes to operate optimally [7]. From Fig. 5, it can be easily seen that ETE is very robust to variation of trapping rate at about 1-ps time scale. In Fig. 6, we also illustrate the robustness with respect to both trapping and reorganization energy (right panel). For rather large values of λ, there are certain regions that are highly robust to both

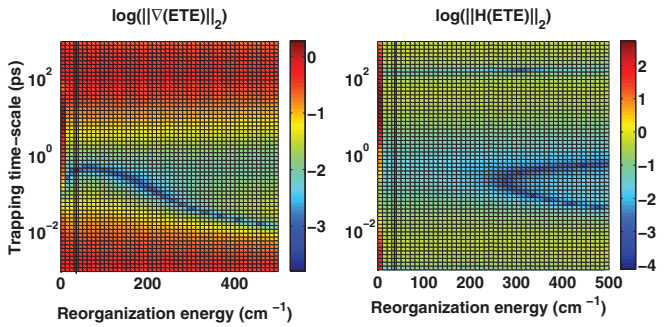

FIG. 6. (Color online) This figure is a complement to Fig. 5 (Left). The degree of ETE optimality is quantified at different values of λ and r_{trap}^{-1} by the norm of the ETE gradient. The dark blue points represent near optimal values. (Right) The degree of ETE robustness is quantified by the Euclidian norm of the ETE Hessian. The blue points represent near robust points. The FMO achieves its maximum efficiency at $r_{\text{trap}}^{-1} = 0.5$ ps. Note that for larger reorganization energies the trapping rate has been increased to achieve optimal ETE. However, this competition does not exist at small and intermediate system-bath coupling strength, where λ is on the order of off-diagonal elements of the FMO free Hamiltonian leading to environment-assisted energy transport. This suggests that a general convergence of time scale might be required to obtain global efficient and robust transport [7].

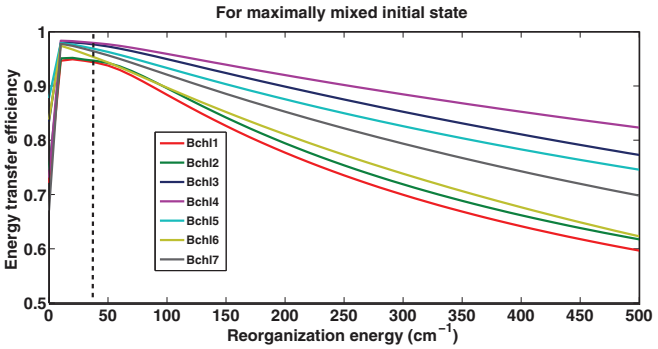

FIG. 7. (Color online) The ETE as a function of reorganization energy for the initially maximally mixed state. In each plot one of the 7 BChls is considered to be connected to the reaction center. BChls 3 and 4 acting as the exciton transfer bridge yield the highest efficiency for almost all values of the reorganization energy. This confirms the experimental evidence that the FMO spatial orientation is such that the BChls 3 and 4 are located near the RC.

parameters, but they are in fact suboptimal, as can be seen from noting their values in the left panel.

To explore the dependence of ENAQT effect on the location of reaction center, we consider the efficiency of other scenarios that the reaction center can be in the proximity of any other BChl sites. Figure 7 shows ETE versus reorganization energy, with a fixed $\gamma = 50\,\mathrm{cm}^{-1}$, for all possible trapping sites. To be unbiased with the respect to the initial state, we assume a maximally mixed initial state. It can be seen that the optimal curves belong to BChls 3 and 4 as expected, since they contribute highly to the lowest energy delocalized excitonic states. It should be noted that optimal environment-assisted quantum transport, and the two extreme regimes of quantum localization can be observed for all of these plots independent of the actual location of trapping. In other words, the behavior of the energy transport efficiency landscape and its dependence on a single governing parameter are not properties of a particular choice of trapping site in the FMO structure.

For completeness, we also investigate the ETE landscape as a function of dissipation (loss) rate and reorganization energy in Fig. 8. In our simulation of the FMO dynamics

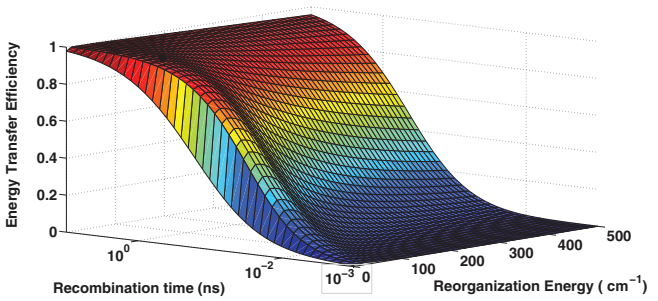

FIG. 8. (Color online) ETE versus dissipation (loss) time-scale r_{loss}^{-1} and reorganization energy. The maximum optimality and robustness for FMO is observed around the estimated value $r_{\mathrm{loss}}^{-1} = 1$ ns, implying the significance of the time-scale separation between dissipation and trapping rates. We note that the ENAQT effect is ubiquitous at all rates of electron-hole recombination process.

we have used the estimated value of $r_{\mathrm{loss}}^{-1} = 1$ ns. In Fig. 8, however, we treat loss rate as a free parameter and we observe that for any stronger dissipation process, ETE would have a suboptimal and less stable behavior. Thus, even if all the other important parameters are within the optimal regime, a large time-scale separation between dissipation and trapping rate is still required to guarantee the highest performance for light-harvesting complexes. Figure 8 also demonstrates that the existence of ENAQT is independent of a particular choice of dissipation rate.

VI. ROBUSTNESS AND OPTIMALITY WITH RESPECT TO PARAMETERS OF FMO HAMILTONIAN

So far, we have demonstrated that for the estimated Hamiltonian elements of the FMO complex, the environmental parameters and trapping rates are within the right set of values leading to an optimal noise-assisted energy transfer efficiency. Moreover, the performance of FMO is robust with respect to variations in such decohering and lossy processes and to uncertainties in initial conditions. However, it is not fully clear if the FMO internal Hamiltonian parameters have evolved to function optimally and fault tolerantly, despite disorders and thermal fluctuations. This issue has been examined for LHCII in Ref. [28] using semiclassical Pauli master equations to simulate the exciton dynamics. Here, we would like to use TC2 to explore how rare the FMO geometry is in terms of its efficiency, whether the specific spatial and dipole moment arrangements of BChls are essential for such highly efficient functioning of this pigment-protein complex, and how robust these parameters are with respect to small and large perturbations in chromophoric distances, dipole moment orientations, and site energy fluctuations. Specifically, we explore if the FMO closely packed structure plays any functional role and illustrate a potentially important convergence of the relevant dynamical time scales in the FMO energy transport. In the following section, we investigate the underlying physical principle of quantum transport in more generic multichromophoric structures beyond the FMO geometry.

The Frenkel exciton Hamiltonian for a multichromophoric system is expressed as

$$H_S = \sum_{j,k} \epsilon_j |j\rangle\langle j| + J_{j,k} |j\rangle\langle k|, \tag{5}$$

in which J_{jk} are Coulomb couplings of the transition densities of the chromophores,

$$J_{jk} \sim \frac{1}{R_{jk}^3}\left[\mu_j \mu_k - \frac{3}{R_{jk}^2}(\mu_j \cdot \mathbf{R}_{jk})(\mu_k \cdot \mathbf{R}_{jk})\right], \tag{6}$$

where $\mathbf{R}_{jk}$ denotes the distance between site j and k, and μ_j is the transition dipole moment of chromophore j [29]. We first study the robustness of free Hamiltonian parameters within the proximity of the estimated values for FMO as given in the Appendix.

A. Robustness of FMO Hamiltonian

Figures 9 and 10 demonstrate the robustness of the FMO structure to variations in its internal parameters. Figure 9

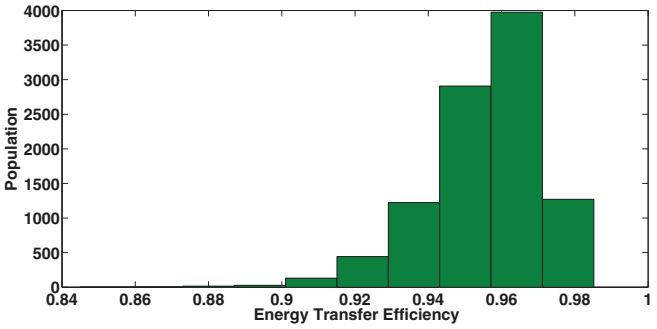

FIG. 9. (Color online) Robustness of FMO transport efficiency with respect to small variations of BChls locations, site energies, and dipole orientations for 10 000 samples: the Hamiltonian parameters are perturbed with site energies disorders of $\pm 10 \mathrm{cm}^{-1}$, dipole-moment uncertainties of $\pm 5^{\circ}$, and BChls spatial displacement of ± 2.5 Å. The statistical distribution of 10^4 random configurations shows a significant degree of robustness such that 99% of samples still preserve an efficiency of above 0.9.

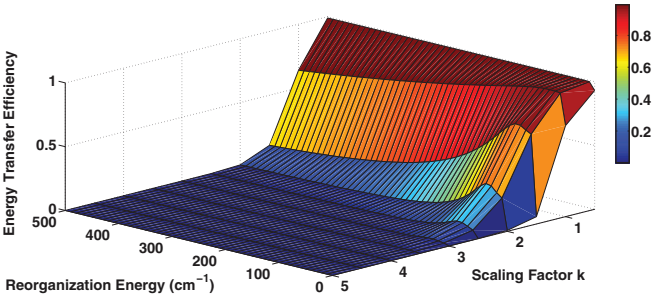

FIG. 11. (Color online) Dependency of ETE on compactness level of the FMO complex. The FMO chromophoric spatial structure is scaled with a factor between 0.5 and 5. The ETE manifold is plotted as a function of the scaling factor and reorganization energy. For all levels of compactness, $\lambda = 30$–$40\,\mathrm{cm}^{-1}$ yields the highest ETE. A more compact complex shows a higher degree of robustness with respect to variation in reorganization energy. The ENAQT behavior can be observed at all levels of compactness, and almost all at the same reorganization energy value.

illustrates that FMO efficiency does not drop drastically with respect to variations in the dipoles orientations, site energies, and Bchls distances close to the neighborhood of the estimated values. Specifically, from 10 000 random samples of FMO with spatial uncertainty around each Bchl location of about ± 2.5 Å, dipole moments orientations variations of $\pm 5^{\circ}$, and site energy static disorder $\pm 10\ \mathrm{cm}^{-1}$, 97% of configurations have efficiency of 95% or higher. This demonstrates a significant degree of robustness with small perturbations. In order to separate the influence of spatial coordinates from angular dipole orientations and disorders, we allow the latter two parameters to take arbitrary values from a large range while keeping Bchl locations uncertainties to be limited by ± 2.5 Å. We observe in Fig. 10 that ETE remains relatively robust with 79% of 10 000 random configurations still having an efficiency of 90% or higher. This is rather counterintuitive considering huge freedom that we have accommodated in the dipole moment arrangements and site energies. These results indicate that spatial degrees of freedom is a dominating geometrical ingredient of the FMO structure and might play a key physical role in its performance. Similar robustness to the FMO system to variation in its structure had been independently reported in Ref. [30].

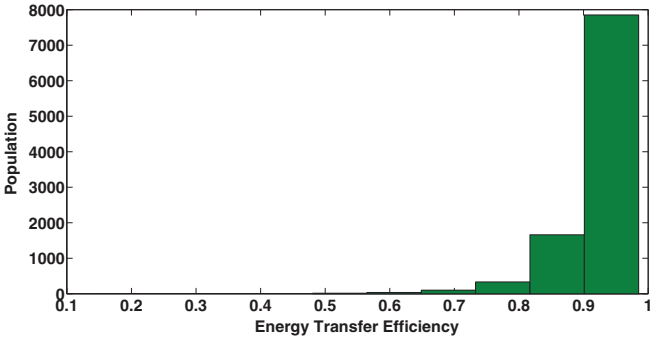

FIG. 10. (Color online) Robustness of the FMO complex transport efficiency with respect to large variations in BChls site energies and dipole moment orientations for 10 000 sample configurations: While the location of BChls are still slightly perturbed, similar to Fig. 9 of about ± 2.5 Å, the dipole moments can take any arbitrary direction and site energy takes any value between zero and $500\,\mathrm{cm}^{-1}$. This Histogram reveals that the relative distance of BChls is playing a crucial role in performance of these random light-harvesting complexes since 79% of them still hold ETE larger than 90%.

B. ENAQT in presence of FMO-size variations

Our results presented in Figs. 9 and 10 clearly indicate that the relative Bchl locations play a major role in the overall performance of the FMO complex. Thus a potentially significant parameter of relevance is the compactness of a given pigment-protein complex. We further explore this feature by introducing a single *compactness* parameter by rescaling the Bchl distances by a factor k. We plot ETE as a function of compactness level k varying by an order of magnitude from 0.5 to 5. To explore any potential interplay of environmental interactions with this particular internal degree of freedom, we also simulate this size-dependent supersession and enhancement of ETE in various reorganization energy, λ, in Fig. 11. It can be seen that although transport efficiency drops significantly by expanding the FMO structure, but the ENAQT phenomenon remains scale invariant for the FMO-like structure.

VII. CONCLUSION

In this paper, we report on robustness properties of ENAQT phenomenon, complementing studies on the role of ENAQT in optimal transport. We considered excitonic energy transfer in FMO complex and presented a comprehensive landscape study of ETE as a function of energy and geometrical parameters representing system and environment degrees of freedom. We found that ENAQT can assist optimal quantum transport to be robust with respect to variations in system-environment parameters. Furthermore, we found that ENAQT has a universal behavior, meaning that it does not disappear when some parameters are outside the optimal regime. The robustness of ENAQT is crucial when designing quantum transport systems

enhanced by bath engineering. Here our observations are based on numerical simulations of one quantum transport system, the FMO complex. It would be interesting and important to perform similar studies for other natural and artificial systems.

ACKNOWLEDGMENTS

We thank J. H. Choi and D. Hayes for helping us with extracting the FMO data. We acknowledge funding from DARPA under the QuBE program (M.M., A.S., S.L., H.R.), ENI (M.M., S.L.), NSERC (M.M.), and NSF (S.L., A.S., H.R.), and ISI, NEC, Lockheed Martin, and Intel (S.L.).

APPENDIX: FMO STRUCTURE INFORMATION

In this work we use the FMO Hamiltonian given in Ref. [31]:

$$H=\begin{pmatrix} 280 & -106 & 8 & -5 & 6 & -8 & -4 \\ -106 & 420 & 28 & 6 & 2 & 13 & 1 \\ 8 & 28 & 0 & -62 & -1 & -9 & 17 \\ -5 & 6 & -62 & 175 & -70 & -19 & -57 \\ 6 & 2 & -1 & -70 & 320 & 40 & -2 \\ -8 & 13 & -9 & -19 & 40 & 360 & 32 \\ -4 & 1 & 17 & -57 & -2 & 32 & 260 \end{pmatrix}.$$

Note that in Ref. [26], it was found through direct calculation that the coupling between BChls 5 and 6 given in Ref. [31] is not correct. For future studies, we recommend using the values reported in Ref. [26].

TABLE I. Spatial location of Bchls and their dipole moment orientation.

Bchl	x (Å)	y (Å)	z (Å)	θ	ϕ
1	28.032	163.534	94.400	0.3816	$-0.6423+\pi$
2	17.140	168.057	100.162	0.067	$0.5209+\pi$
3	5.409	180.553	97.621	0.1399	$1.3616+\pi$
4	9.062	187.635	89.474	0.257	$-0.6098+\pi$
5	21.823	185.260	84.721	−0.1606	$0.6899+\pi$
6	23.815	173.888	82.810	−0.4214	$-1.4686+\pi$
7	12.735	174.887	89.044	0.578	$-1.0076+\pi$

Table I gives the estimated values of dipole moment orientations and positions of Bchls, extracted from the pdb file of the FMO complex [32].

The FMO interchlorophyll coupling is dipole-dipole interaction

$$J_{jk}=\frac{C}{R_{jk}^3}\left[\mu_j\mu_k-\frac{3}{R_{jk}^2}(\mu_j\cdot\mathbf{R}_{jk})(\mu_k\cdot\mathbf{R}_{jk})\right], \quad \text{(A1)}$$

for which we consider the constant $C|\mu|^2 = 134\,000\ \mathrm{cm}^{-1}\mathrm{Å}^3$ [26].

[1] V. May and O. Kuhn, *Charge and Energy Transfer Dynamics in Molecular Systems* (Wiley-VCH, Weinheim, 2004).
[2] S. Datta, *Quantum Transport: Atom to Transistor* (Cambridge University Press, Cambridge, 2005).
[3] *Quantum Effects in Biolgy*, edited by M. Mohseni, Y. Omar, G. Engel, and M. Plenio (Cambridge University Press, Cambridge, UK, 2014).
[4] M. Mohseni, P. Rebentrost, S. Lloyd, and A. Aspuru-Guzik, J. Chem. Phys. **129**, 174106 (2008).
[5] P. Rebentrost, M. Mohseni, and A. Aspuru-Guzik, J. Phys. Chem. B **113**, 9942 (2009).
[6] P. Rebentrost, M. Mohseni, I. Kassal, S. Lloyd, and A. Aspuru-Guzik, New J. Phys. **11**, 033003 (2009).
[7] M. Mohseni, A. Shabani, S. Lloyd, and H. Rabitz, J. Chem. Phys. **140**, 035102 (2014).
[8] M. B. Plenio and S. F. Huelga, New J. Phys. **10**, 113019 (2008).
[9] F. Caruso, A. W. Chin, A. Datta, S. F. Huelga, and M. B. Plenio, J. Chem. Phys. **131**, 105106 (2009).
[10] A. Olaya-Castro, C. F. Lee, F. F. Olsen, and N. F. Johnson, Phys. Rev. B **78**, 085115 (2008).
[11] A. W. Chin, J. Prior, R. Rosenbach, F. Caycedo-Soler, S. F. Huelga, and M. B. Plenio, Nat. Phys. **9**, 113 (2013).
[12] E. J. O'Reilly and A. Olaya-Castro, Nature Commun. **5**, 3012 (2014).
[13] G. S. Engel, T. R. Calhoun, E. L. Read, T. K. Ahn, T. Mancal, Y. C. Cheng, R. E. Blankenship, and G. R. Fleming, Nature **446**, 782 (2007).
[14] H. Lee, Y.-C. Cheng, and G. R. Fleming, Science **316**, 1462 (2007).
[15] G. Panitchayangkoon, D. Hayes, K. A. Fransted, J. R. Caram, E. Harel, J. Wen, R. E. Blankenship, and G. S. Engel, Proc. Natl. Acad. Sci. USA **107**, 12766 (2010).
[16] A. F. Fidler, J. R. Caram, D. Hayes, and G. S. Engel, J. Phys. B **45**, 154013 (2012).
[17] D. Hayes and G. S. Engel, Philos. Trans. R. Soc. A **370**, 3692 (2012).
[18] A. Shabani, M. Mohseni, H. Rabitz, and S. Lloyd, Phys. Rev. E **86**, 011915 (2012).
[19] M. Mohseni, A. Shabani, S. Lloyd, Y. Omar, and H. Rabitz, J. Chem. Phys. **138**, 204309 (2013).
[20] J. Gilmore and R. H. McKenzie, J. Phys. Chem. A **112**, 2162 (2008).
[21] J. Wu, F. Liu, Y. Shen, J. Cao, and R. J. Silbey, New J. Phys. **12**, 105012 (2010).
[22] T. Ritz, S. Park, and K. Schulten, J. Phys. Chem. B **105**, 8259 (2001).
[23] A. Ishizaki and G. R. Fleming, Proc. Natl. Acad. Sci. USA **106**, 17255 (2009).
[24] B. Cui, X. X. Yi, and C. H. Oh, J. Phys. B **45**, 085501 (2012).
[25] H. W. Remigy, H. Stahlberg, D. Fotiadis, B. Wolpensinger, A. Engel, G. Hauska, and G. Tsiotis, J. Mol. Biol. **290**, 851 (1999).
[26] J. Adolphs and T. Renger, Biophys. J. **91**, 2778 (2006).
[27] J. Wen, H. Zhang, M. L. Gross, and R. E. Blankenship, Proc. Natl. Acad. Sci. U.S.A. **106**, 6134 (2009).
[28] M. K. Sener, D. Lu, T. Ritz, S. Park, P. Fromme, and K. Schulten, J. Phys. Chem. B **106**, 7948 (2002).
[29] X. Hu, T. Ritz, A. Damjanović, and K. J. Schulten, Phys. Chem. B **101**, 3854 (1997).
[30] S. Jesenko and M. Znidaric, New J. Phys. **14**, 093017 (2012).
[31] M. Cho, H. M. Vaswani, T. Brixner, J. Stenger, and G. R. Fleming, J. Phys. Chem. B **109**, 10542 (2005).
[32] The FMO PDB file was provided by M. Cho laboratory.